Insights into processes and consequent metal(loid) behavior in dredged estuarine sediments upon electrokinetic treatment

Hussein J Kanbar, Mohamed-Tahar Ammami, Ahmed Benamar

Environmental Challenges 15 (2024) 100880

Contents lists available at ScienceDirect

Environmental Challenges

journal homepage: www.elsevier.com/locate/envc

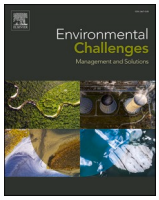

Insights into processes and consequent metal(loid) behavior in dredged estuarine sediments upon electrokinetic treatment

Hussein J. Kanbar *, Mohamed-Tahar Ammami, Ahmed Benamar

Laboratoire Ondes et Milieux complexes (LOMC), UMR 6294 CNRS, University of Le Havre Normandy (ULHN), 76600, Le Havre, France

ARTICLE INFO

Keywords:
Circular economy
Dredged sediment treatment
Environmental sustainability
Remediation
Reconstructed soil

ABSTRACT

The use and reuse of natural and waste materials after treatment has become increasingly crucial as a means of achieving sustainable and environmentally-friendly solutions, and is part of a broader trend towards embracing circular economy principles. This study aims to understand the behavior of different elements (metal(loid)s and non-metals) and minerals during and after electrokinetic remediation (EKR) and to develop an effective approach to monitor its progress and overcome unwanted occurrences. In this regard, estuarine sediments, collected from Tancarville (Seine River estuary, France), were electrokinetically treated using a 64 L laboratory reactor; treatment was done 8 h per day for 21 days. The physico-chemical properties (pH, electric conductivity, and oxido-reduction potential) and current were monitored during treatment. The spatial evolution of the physico-chemical, physical (grain size distribution), mineral (mainly carbonates), organic, and elemental (As, Ca, Cl, Mg, Na, Pb, Sr, Zn, and Zr) characteristics was studied to assess the treatment efficiency. The results showed that the acidic conditions in the anodic sediments caused the dissolution of carbonates (calcite, dolomite, and aragonite), resulting in a considerable reduction in As, Zn, and Pb. Additionally, Cl as well as electric conductivity were significantly reduced from most sediments, which is essential in agricultural practices. Furthermore, materials had precipitated and settled in the anolyte and catholyte chambers, which acted as sorbents for elements that were released from the sediments (mainly Zn and As). Finally, three distinct phases occurred during treatment and were mainly linked to the current intensity and electric conductivity on the one hand, and the dissolution of carbonates and metal(loid) release on the other. This approach can be used to treat sediments and other media to improve the overall efficiency of remediation processes and create an end product with desired characteristics.

1. Introduction

The awareness of environmental concerns necessitates a transition towards a more sustainable environment. Such concerns can be overcome by reducing waste production and re-formulating waste materials into usable ones. Indeed, the European Union (EU) promotes the shift towards a circular economy by laying down measures to reduce and manage waste materials. Sediments, regardless of their hazardous level or condition, are considered waste materials once dredged (EU, 2008a), and therefore require treatment before use. However, the EU Waste Framework Directive (2008/98/EC) does not directly apply to dredged sediments. There are further restrictions on using dredged sediments in the agricultural sector (EU, 2019; Macci et al., 2022). Nonetheless, the EU has developed specific regulations for the management of dredged sediments (EU, 2008a, 2008b, 2000). These regulations aim to ensure that the dredging activities are carried out in an environmentally sustainable manner. Additionally, the EU has developed networks in which stakeholders and experts guide the sustainable management of dredged sediments (SedNet, 2004). These guidelines provide recommendations on the management and disposal of dredged sediments and promote the reuse and recycling of sediments whenever possible. In Europe, between 100 – 200 million m^3 of sediments are annually dredged (Bose and Dhar, 2022; SedNet, 2004). Unfortunately, a large fraction is dumped in open sea or transferred to fill-in basins (e.g., Apitz, 2010). Alternatively, dredged sediments can be used in construction materials (e.g., bricks and concrete), road materials (e.g., base and sub-base), and agriculture (e.g., amendment and fertilizer) (e.g., Apitz, 2010; Interreg ReCon Soil, 2022; Mesrar et al., 2021; Renella, 2021).

In the framework of reaching a sustainable environment and reusing waste materials, the “ReCon Soil” project (Interreg France – channel –

* Corresponding author.
E-mail address: hsen.kanbar@gmail.com (H.J. Kanbar).

https://doi.org/10.1016/j.envc.2024.100880
Received 20 November 2023; Received in revised form 13 February 2024; Accepted 26 February 2024
Available online 1 March 2024

England) aims to incorporate treated waste materials, such as dredged sediments and quarry sludge, into agricultural soils (named reconstructed soils); thus overcoming soil shortage and soil degradation (Interreg ReCon Soil, 2022). The work presented in this paper is part of the ReCon Soil project. Sediment amendments in agricultural soils can improve soil quality. For example, fine sediments that are rich in clay minerals can be used as nutrient sources and increase carbon sequestration and water holding capacity, organic matter (OM)-rich sediments can overcome OM-depleted soils and improve water holding capacity as well, and carbonate-rich sediments can improve buffering capacity (e.g., Churchman et al., 2020; Kiani et al., 2021). Those components can also improve aggregation properties due to their cohesive character (Grabowski et al., 2011). Nonetheless, sediments can also be rich in trace elements that are potentially toxic to plants (Ferrans et al., 2022; Vácha et al., 2011); metal(loid)s such as Pb, Zn, Cu, and As can accumulate in plants and render them inedible (Hahn et al., 2022; Zhang et al., 2013). Therefore, adequate sediment treatment is required before reuse in agriculture or other fields (e.g., as construction materials). Among the efficient treatment methods is electrokinetic remediation (EKR or EK for electrokinetics). Indeed, EKR has been used to treat sediments and soils and is particularly efficient in treating fine materials (e.g., Ammami et al., 2015; Betremieux and Mamindy-Pajany, 2022; Chen et al., 2020; Han et al., 2021; Song et al., 2016; Wen et al., 2021). However, certain elements, such as Ca and Mg (macro-nutrients), are beneficial to plants and are not targeted during sediment treatment (Kiani et al., 2021). For example, acidic conditions induced by EKR enhance the mobility of potentially toxic elements (e.g., Pb, Zn, and Zr), but can also dissolve carbonate minerals and cause the release of Ca and Mg. Consequently, the buffering capacity of the treated sediment is reduced and becomes more vulnerable to acidification.

The principle behind EK and the parameters that enhance remediation are discussed elsewhere (e.g., Acar and Alshawabkeh, 1993; Ammami et al., 2022, 2015; Cameselle et al., 2013; Han et al., 2021; Song et al., 2016; Wen et al., 2021). This study focuses on treating dredged sediments, subsequently employed in the reconstruction of soils for agricultural practices (Interreg ReCon Soil, 2022). In the case of estuarine (and marine) sediments, salts (e.g., halite, NaCl) and metals need to be reduced since they negatively affect plant growth (Ferrans et al., 2022; Tian et al., 2020; Vácha et al., 2011); electric conductivity (EC) is correlated to salinity and therefore can be used as a proxy to follow salinity (e.g., Gorji et al., 2020). In addition to its direct negative effect on plants, salts increase metal mobility and uptake by plants (Acosta et al., 2011; Du Laing et al., 2008, 2007). Salts and metals can also be removed by other techniques, such as phytoremediation. However, phytoremediation is generally a slow process and takes years (e.g., Sordes et al., 2023), whereas EKR is relatively fast and efficient results are obtained within a few days to weeks (e.g., Ammami et al., 2013, 2022; Han et al., 2021). During EKR, acidic fronts usually form in sediments (or other media) in the anodic zone due to water oxidation, the release of H^+, and its migration toward the cathodic zone (Selvi et al., 2019; Wen et al., 2021). Indeed, acidic conditions enhance the desorption, and thus removal or reduction of metals through the formation of metal ionic species, competition with H^+, and alteration of surface charge (Beyrami, 2021; Caporale and Violante, 2016; Carrillo-González et al., 2006). Furthermore, acidic conditions promote Fe and Mn oxi-hydroxide precipitation and carbonate dissolution; the former can sorb metals during precipitation and the latter releases associated metals (Lynch et al., 2014). The opposite is also true, metals might be sorbed during the precipitation of carbonates in alkaline conditions (Elzinga et al., 2006; Elzinga and Reeder, 2002), thus resulting in reduced remediation efficiency (Ouhadi et al., 2010). Alkaline conditions form in the cathodic zone due to water reduction and the release of OH^-; this alkaline front then migrates away from the cathode. Citric acid has been proven to be an efficient and eco-friendly ligand in EKR due to its ability to bind metal cations in most pH ranges (e.g., Ammami et al., 2015; Kanbar et al., 2023; Song et al., 2016; Wen et al., 2021).

The efficiency of EKR does not merely rely on the reduction of metal (loid)s (or other unwanted elements such as As, Cl, Na, Sr, Pb, Zn, and Zr) and the preservation of wanted elements and minerals (such as Ca, Mg, and carbonates), but on understanding the processes that govern the behavior of metals and minerals. By gaining a thorough understanding of these processes, researchers and practitioners can optimize the remediation approach to be more efficient in terms of energy-cost and end product, as well as tailor the remediation medium to best suit its intended application (e.g., agriculture). Therefore, the aims of this study are twofold. Firstly, to gain a comprehensive understanding of the behavior of different elements (metal(loid)s and non-metals) during EKR, including their mobility in the environment, their relationship with various physico-chemical parameters (pH, oxido-reduction potential "ORP", and electric conductivity), and their potential impact on carbonate dissolution. Secondly, the study aims to develop an effective approach for monitoring the progress of EKR and identify and mitigate potentially unwanted occurrences. This approach can be adapted for use in other environmental matrices to improve the overall efficiency of remediation technologies.

2. Materials and methods

2.1. Sediment collection, laboratory reactor, and running parameters

Estuarine sediments were collected from Tancarville (upper estuary of the Seine River, France) during a dredging operation. Sediments are regularly dredged to maintain optimal water levels, ensuring secure ship navigation. Approximately 7 million m^3 of sediments are annually dredged from the estuary area of Le Havre and Rouen ports (Mesrar et al., 2021), located downstream of the sampling site. As a result, an experimental land deposit of approximately 5 ha (50,000 m^2) contains tons of sediments that have been stored in Tancarville for over 13 years. Although vegetation has flourished in that area (Benamar et al., 2024), the deposited sediments remain with no practical use (e.g., Bose and Dhar, 2022). The collected sediments were homogenized before filling the EKR experimental reactor. The reactor is detailed in Kanbar et al. (2023). The original reactor includes two sediment compartments. In this study, only one of the two compartments was used since the two compartments were statistically proven to be replicates (Kanbar et al., 2023). Briefly, the 64 L sediment compartment has 40 × 40 × 40 cm dimensions (Fig. 1). Perforated plates with geotextile filters were positioned between the sediment compartment and the electrolyte chambers. The characteristics of the sediment are summarized in Table 1 (more details on the methods are included in later sections).

The EK treatment was periodically run for 21 days (8 hrs ON and 16 hrs OFF) using a 40 V (i.e., 1 V/cm) direct current (DC). The current was applied only for 6 hrs in the first two days to avoid overheating. Citric

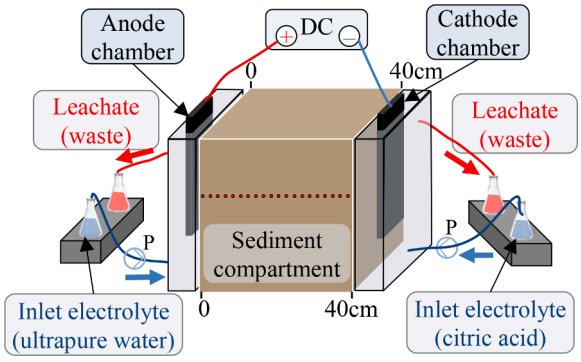

Fig. 1. The 64 L electrokinetic remediation reactor. The circular shapes in the sediment compartment mark where the direct physico-chemical measurements (pH, EC, and ORP) were collected along the anode – cathode direction. P: pump, DC: direct current generator.

Table 1
Characteristics of the dredged sediment. The average values from 4 technical replicates with standard deviations are presented.

		Mineral composition (%)	
pH	7.4 ± 0.1	Quartz	27.4
EC (mS/cm)	21.3 ± 1.1	Calcite	28.6
D_{50} (μm)	13.8 ± 0.1	Illite	15.2
Clay (%)	5.2 ± 0.5	Kaolinite	7.3
Silt (%)	87.4 ± 1.2	K-feldspar	3.5
Sand (%)	7.4 ± 0.7	Albite	4.6
LoI_{550} or OM (%)	10.5 ± 0.6	Dolomite	3.9
Carbonates (%)	31.3 ± 0.1	Aragonite	2.5
Water content (%)	63.1 ± 1.3	Smectite	2.0
ORP (mV)	19.5 ± 5.3	Amphibole	2.0
		Others	2.9

EC: electric conductivity
LoI_{550}: loss on ignition at 550 °C
OM: organic matter
ORP: oxido-reduction potential

acid (CA, 0.1 M, 2.36 pH, and 3.2 mS/cm electric conductivity "EC") was used as electrolyte in the cathode chamber. Ultrapure water was used in the anode chamber. Peristaltic pumps were initially set at 10 ml/hr flow rate to supply the chambers with electrolytes. However, electrolytes as well as water in the sediment compartment evaporated as a result of elevated temperatures, especially in the first days; consequently, the electroosmotic flow could not be calculated. So, the electrolyte chambers were filled daily and their levels were maintained to keep the sediments well-saturated with the electrolytes.

2.2. Monitoring electric current and physico-chemical parameters of the anode and cathode chambers during treatment

The electric current as well as the physico-chemical parameters, i.e., pH, EC, and ORP of the electrolyte chambers, were monitored during the 21-day treatment. Two measurements were taken daily, one at the start and another at the end of the daily 8 hr electric current application (named start and end, respectively). A multimeter (HI5521) equipped with HI76312 (EC) and HI1131 (pH) electrodes was used to measure the EC and pH in the electrolyte chambers, respectively; the temperature was monitored using a temperature probe. A combined platinum-Ag/AgCl redox electrode (HI4430B, from HANNA instruments) was used for ORP measurements.

2.3. Direct physico-chemical analyses after treatment

At the end of the 21-day experiment, the surface sediment layer was removed due to differences in conditions in comparison to the subsurface; indeed, the contact with atmospheric oxygen caused the precipitation of some phases (this will be discussed later in the text). Although the uniqueness of this layer is only a few mm deep, the top 2 cm layer was removed. Subsequently, direct pH, EC, and ORP measurements were taken at a 2 cm interval in the anode – cathode direction (Fig. 1). A portable pH meter (HI99121, from HANNA instruments) with a spear-tipped pH electrode (HI12923) and a FieldScout Direct Soil EC Meter (Spectrum Technologies) were used for direct pH and EC measurements, respectively. The ORP was directly measured using the same equipment as stated above (Section 2.2).

2.4. Sediment characterization after treatment

Based on the direct physico-chemical parameters (Section 2.3), sediment sections were collected along the anode – cathode direction for further analyses. Most sediment sections were 2 cm thick, but sections with similar findings were grouped (e.g., 16 – 18 cm and 18 – 20 cm sediments were grouped into one section, i.e., 16 – 20 cm). Two samples were collected from each section (replicates) and centrifuged for 20 min at 4500 rpm (4640 g or 205 RAD). The extracted porewater (PW) samples were then used to measure pH, EC, and ORP (same equipment as stated in Section 2.2); these measurements (named indirect) were compared with the direct measurements. The settled sediments were then frozen and freeze-dried for later analyses; however, a fresh sample was stored at 4 °C for grain size distribution (GSD) analysis. The freeze-dried samples were then ground using an agate mortar and pestle. The water content of the same samples was determined from the mass loss between the initial (i.e., before centrifugation) and final samples (after freeze-drying). The methods for GSD, mineralogy, organic matter (OM), carbonates, and elemental composition determination are detailed elsewhere (Kanbar et al., 2023). Briefly, the GSD and particle percentiles (D_{10}, D_{50}, and D_{90}) were determined using a Mastersizer 2000 with a Hydro 2000MU dispersion unit (Malvern Instruments), mineralogy was determined using a PANalytical X'pert powder X-ray diffraction (XRD) instrument (λ CoK_{α} = 1.78901 Å) and quantified using Profex-BGMN (Döbelin, 2021; Doebelin and Kleeberg, 2015; Post and Bish, 1989), organic matter was quantified by the loss on ignition (LoI) method (Heiri et al., 2001), total carbonates were quantified using the volumetric calcimeter method (ISO 10693, 1995), and elemental composition was determined using X-ray fluorescence spectroscopy (XRF Xepos - AMETEK) at PLATIN' (PLATeau d'Isotopie de Normandie) core facility (Caen, France); the geological reference material BE-N (basalt), issued by GIT-IWG (Groupe International de Travail ou International Working Group), was used as the calibration standard (Govindaraju, 1989; SARM, 2015). In this study, we report the contents of elements that can be beneficial to plants (i.e., Ca and Mg, which are macro-nutrients), elements that indicate salinity (i.e., Na and Cl), and potentially toxic metal(loid)s for plants (i.e., As, Pb, Zn, and Zr). The limits of detection (LOD) and quantification (LOQ) for the quantified elements (in mg/kg) are as follows: Na (100 and 295), Cl (20 and 30), Mg (100 and 180), Ca (100 and 285), Sr (2 and 20), Zn (10 and 20), As (0.1 and 1), Zr (2 and 20), and Pb (1.0 and 10). The contents of the initial sediment were above the LOQ. The measured contents for Na, Mg, Cl, Ca, Zn, Sr, and Zr lied within the confidence interval (95%) of the certified reference material (BE-N). The average measured content (± standard deviation), theoretical value, and confidence interval (95%) for Na (%) were 2.2 ± 0.1, 2.4, and 2.2 – 2.5, for Mg (%) were 8.1 ± 0.1, 7.9, and 7.7 – 8.5, for Cl (mg/kg) were 280 ± 7, 300, and 276 – 324, for Ca (%) were 9.8 ± 0.1, 9.9, and 9.7 – 9.9, for Zn (mg/kg) were 110.7 ± 0.7, 120.0, and 108.2 – 131.8, for Sr were 1372 ± 4, 1370, and 1358 – 1386, and for Zr were 279 ± 2, 265, and 247 – 284, respectively. As for As and Pb, the measured values deviated from the standard material and therefore were corrected by fitting them to the theoretical values.

2.5. Precipitated and settled materials in the anode and cathode chambers

Interestingly, settled materials were noticed in the anode and cathode chambers after treatment. These materials surely formed and precipitated in the chambers and were not mobilized from the sediment compartment since the electrolyte chambers were separated from the sediment compartment by geotextile membranes that allow only dissolved phases to pass through. These materials, named settled anode (SA) and settled cathode (SC), were analyzed similarly to the sediments.

2.6. Statistical analysis

Principal component analysis (PCA) was used to transform the large set of variables into smaller ones (using IBM SPSS Statistics Version 25.0), thus facilitating the analyses and interpretation of the data. Varimax rotation was applied to link the variables to their respective principal components (PCs). Indeed, PCA is commonly used to delineate, interpret, and understand environmental data (e.g., Micó et al., 2006). We used PCA to show the significance of the temporal variation of the physico-chemical and electric parameters during EKR and to obtain correlations between the sediment's components (elemental, mineral,

and organic) after treatment.

3. Results

3.1. Temporal evolution of electrical parameters and energy consumption

A significant temperature increase was expected during the first few days of treatment since the sediment has high resistance. Indeed, and to avoid overheating of the sediment, the power was periodically paused during the first two days and only 6 h, instead of 8, were applied. This step was unnecessary when similar sediments were treated using a 0.5 V/cm voltage gradient instead of 1 V/cm (Kanbar et al., 2023). Anyway, the current gradually increased during the first five days (Fig. 2a). Under a constant voltage gradient, as in this case, the current increase reflects a decrease in global resistance, which in turn indicates higher conductive elements present in the system. This increase in EC comes mainly from generating conductive species in the anode and cathode chambers as well as in the porewater. Indeed, water oxidation at the anode and reduction at the cathode release H^+ and OH^-, respectively; furthermore, the EC increase is also linked to the liberation of conductive species from the sediment (particle surface) to the porewater. The current then gradually decreased after day 5 (Fig. 2a), with a relatively low decrease rate at days 11 – 12. It is worth noting that the daily current variation showed a steady decline starting from day 5 (i.e., the difference between the daily end and starting current); the daily variation became insignificant on the last day of treatment. The decline in current from the end of a day to the start of the next is due to the removal of species from the porewater and their translocation to electrolyte chambers by diffusion and osmosis. Indeed, applying intermittent current promotes the reduction of ionic species (e.g., Ammami et al., 2015; Benamar et al., 2019; Micic et al., 2001).

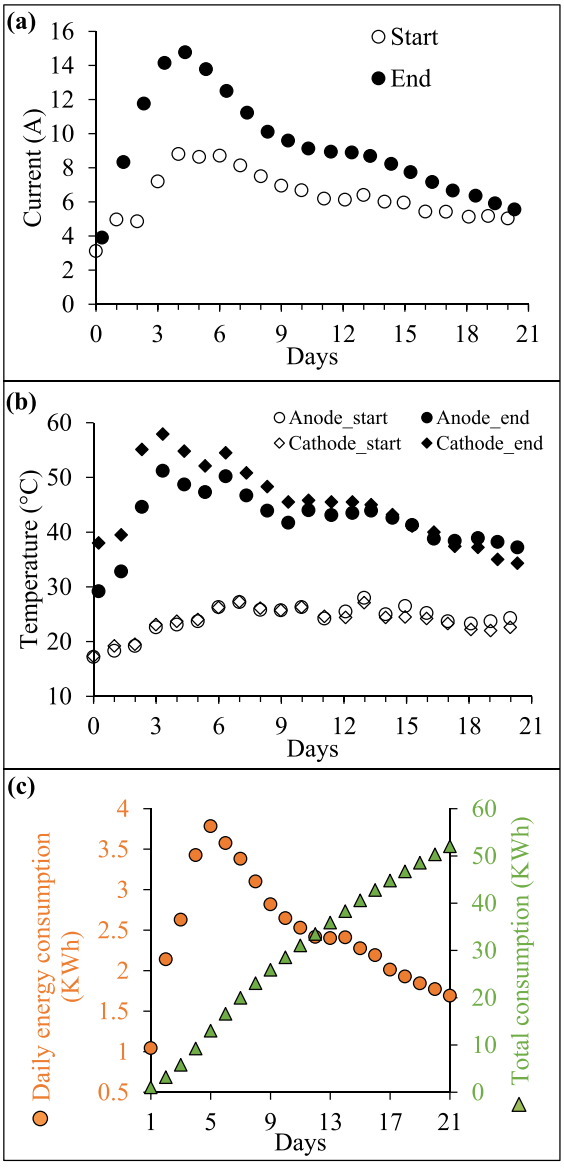

Fig. 2. The temporal evolution of a) current (ampere "A") and b) temperature (°C) in the anode and cathode chambers as a function of time. Values were recorded at the start (daily starting) and end (daily final) of the daily 8 hr experiment. c) The daily and total energy consumption during treatment (KWh).

The temperature in the anode and cathode chambers followed a trend similar to the current. The daily starting temperature varied since it was not controlled during the experiment and because it was affected by the final temperature that was reached on the previous day (Fig. 2b). However, the daily starting temperatures in the anode and cathode chambers were comparable. The effect of ionic species in those chambers (mainly H^+ in the anode and OH^- in the cathode) on the temperature could only be noticed after applying a DC voltage (daily end temperatures in Fig. 2b). The daily end temperatures of the cathode were higher than those of the anode for the first 11 – 12 days. This is partially due to the higher ionic conductance of H^+ (34.9 $mS.m^2/mol$) that is produced in the anode chamber, in comparison to that of OH^- (19.8 $mS.m^2/mol$) that is produced in the cathode chamber (Vanysek, 1993); indeed, more heat is generated in the cathode chamber due to the higher resistance (lower EC) of OH^- in comparison to H^+. The daily variation in temperature, similar to the current, decreased after 11 – 12 days (Fig. 2b).

The daily energy consumption gradually increased and reached a maximum of ~3.8 KWh at the end of the 5th day (Fig. 2c). This increase is explained by the increase in conductive species (as described in the previous paragraphs). Then the daily energy consumption gradually decreased until a quasi-stable phase formed during days 12 – 14 (average of 2.41 ± 0.01 KWh), which was followed by another decline until day 21 (1.7 KWh). In total, 52 KWh was consumed (equivalent to 406.6 KWh/m^3 or 0.339 KWh/kg), which is slightly higher than other studies with similar conditions (e.g., Kim et al., 2012; Zhao et al., 2022). This is partially due to higher current levels, which improve the remediation efficiency at the expense of higher energy consumption (Han et al., 2021; Xue et al., 2017).

3.2. Temporal evolution of physico-chemical parameters: EC, pH, and ORP

The electric conductivity in the anode and cathode chambers mainly increased during the first 8 to 9 days (Fig. 3a). The higher conductivity in the anode chamber, as explained in Section 3.1, is due to the higher ionic conductance of H^+; the mobility of citrate towards the anode can also explain the relatively high EC. There was a quasi-stable phase between days 5 and 7, which had comparable daily end EC values and relatively lower EC daily variations in both electrolyte chambers. The EC then significantly increased at the end of day 8 in both chambers (by ~35 mS/cm). After that point, the daily EC change in the anode chamber was insignificant and remained quasi-stable until day 15 when it gradually decreased. The daily EC variation in the cathode chamber fluctuated after day 8, and the daily end EC showed a slight decrease until day 17 and was quasi-stable for the remaining days. The minor EC decline in both chambers after day 8 – 9 and the clear EC decline after day 15 suggest that fewer conductive species are present in the chambers, which might be caused by the precipitation of phases. Furthermore, the decrease in EC overnight indicates the removal of ionic species (Section 3.1) or the precipitation of phases.

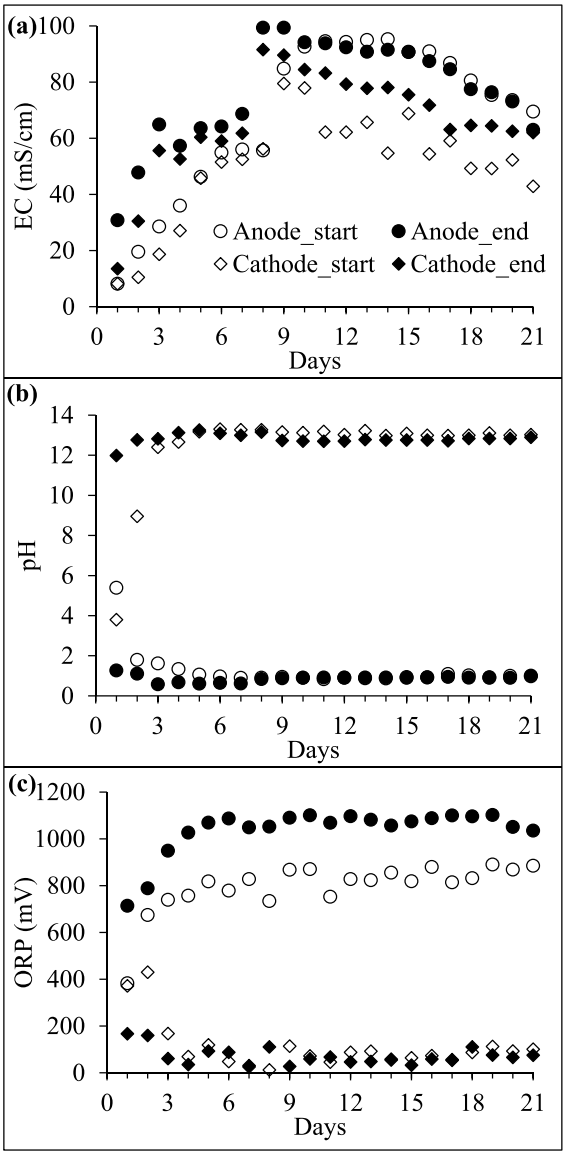

Fig. 3. The variation of a) EC (mS/cm), b) pH, and c) ORP (mV) of the anode and cathode chambers during treatment.

The pH variation reflects the production of H^+ and OH^- in the anode and cathode chambers, respectively (Fig. 3b). The anode showed a relatively fast drop in pH, despite the high carbonate contents and therefore high buffering capacity of the sediment (Table 1). The rise in pH in the cathode chamber took a longer time in comparison to the pH change in the anode, which might be partially explained by the presence of CA in this chamber, which can counteract the pH rise. The daily pH variation in the anode chamber was only visible during the first 7 days, while there was always a variation, even a slight one, in the daily pH values in the cathode chamber. This pH variation, the decline in EC after day 8 – 9 (Fig. 3a), and the noticeable daily EC variation in the cathode chamber further support that reactions occurred in the cathode chamber, which can be precipitation and/or dissolution, but predominated by the first.

The generation of oxic (O_2 release) and reducing conditions in the anode and cathode chambers, respectively (Fig. 3c), explain the ORP variation (Ammami et al., 2020). Indeed, water oxidation and the continuous release of O_2 in the anode chamber reflected increasing ORP values until day 5. However, the daily ORP variation remained throughout the 21 days; this variation was more obvious in the anode chamber. Oxygen accumulated in the anolyte chamber during treatment, despite the relatively high temperature, while it declined overnight as shown by reduced ORP (i.e., starting values in Fig. 3c). As for the cathode chamber, the decline was relatively fast and the daily variation was insignificant when compared to that of the anode chamber. Therefore, the daily ORP variation in the anode chamber suggests that processes other than H^+ introduction occurred, probably linked to the interaction with sediment components. In general, the daily final ORP values averaged 1074 ± 23 mV and 63 ± 25 mV in the anode and cathode chambers, respectively.

3.3. Spatial distribution of physico-chemical properties in the sediments after treatment

The production of H^+ and OH^- in anode and cathode chambers, respectively, and their migration toward the opposite electrodes cause a pH decline in the anodic sediments and a pH rise in the cathodic sediments. Firstly, the direct and indirect (from PW after centrifuge) pH measurements showed similar values and trends throughout most sections, except in the 17–23 cm region (Fig. 4a). The pH transition was better visualized in the PW samples as these values reflect the pH of sediment sections (slices) instead of point measurements (i.e., 20–22 cm and 22–24 cm instead of 21 and 23 cm, respectively). Nonetheless, direct pH measurements are more accurate than those measured in PW since reactions can occur in the latter (i.e., starting from sampling, centrifugation, and actual measurement), such as dissolution or precipitation of minerals (e.g., Lynch et al., 2014; Vicente et al., 2022). The pH showed three distinct phases along the anode – cathode direction, which can be seen by strongly acidic, slightly acidic to neutral, and alkaline pH values in the 0–4 cm, 7–20 cm, and 22–40 cm sediments, respectively. The overall pH was higher (8.1) than the initial sediment (7.4). The final pH was derived by considering the pH values of each section (across the anode – cathode direction) and taking into account the thickness of each respective section; the same approach was used to calculate the final EC and ORP values. The pH of the materials that settled in the anode (SA) and cathode (SC) chambers were 3.7 and 11.1, respectively, reflecting the chambers' pH conditions. Furthermore, SA and SC did not have the same pH values as the respective nearby sediment sections (i.e., 0 – 2 cm for SA and 38 – 40 cm for SC).

The difference in EC between the PW and direct measurements was more prominent in comparison to the pH; however, the values were similar for the 20–40 cm sediments (Fig. 4b). The difference can be attributed to the reactions that could have happened after sampling (before centrifugation), during centrifugation, and before EC measurement from the PW. Higher EC values for PW, mainly in the 0–15 cm sediments, suggest that more conductive species are present in comparison to the sediments before they were sampled. This can be explained by the dissolution of phases and the liberation of ions caused by centrifugation (e.g., salts and gypsum). The EC was significantly reduced in the 15 – 35 cm sediments, while other sediments had values above the final EC (5.8 mS/cm) and below the initial EC (21.3 mS/cm). Nonetheless, the final EC was significantly reduced by more than 70.2 %. The SA and SC had EC values comparable to the 0–2 cm and 38–40 cm sediments (~18 mS/cm).

The ORP showed a typical gradient from the anode to the cathode (Fig. 4c). High and low ORP values in the anodic and cathodic zones are caused by the oxic and anoxic conditions, respectively. The sediments are further oxidized after sampling due to the contact with atmospheric oxygen and due to centrifugation, thus explaining higher ORP for the PW samples. This highlights the importance of measuring the physico-chemical properties directly from the sediments. The final ORP was slightly higher than that of the initial sediment. The ORP of the SA and SC samples were similar to the 0–2 cm and 38–40 cm sediments, respectively.

The water content was highest in the 0–6 cm sediments (63.8 % ± 0.9%) and comparable to the initial water content (Fig. 4d and Table 1).

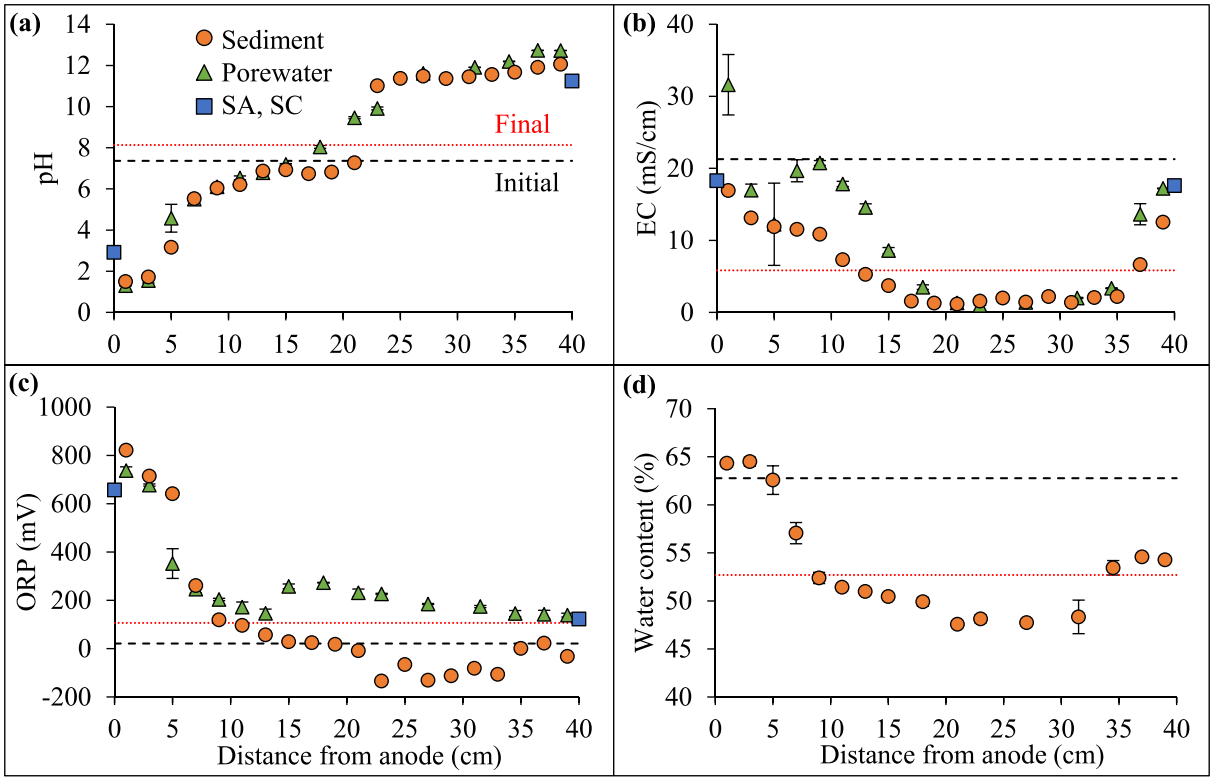

Fig. 4. The spatial variation of a) pH, b) EC (mS/cm), c) ORP (mV), and d) water content (%) of the sediment sections and the settled materials (SA and SC) at the end of the experiment. The averages are reported for the PW samples (a – c) and the water content (d), with standard deviations as vertical error bars. For comparison, the initial (dashed) and final (dotted) values are plotted.

The water content then significantly dropped until 10 cm away from the anode. In the 10–16 cm region, there was only a slight decrease in water content and the 20–30 cm and 33–40 cm sediments showed quasi-stable water contents. Although the electroosmotic flow was not measured, the movement of water molecules largely depends on the formation of hydration spheres with species present in the porewater (e.g., Mähler and

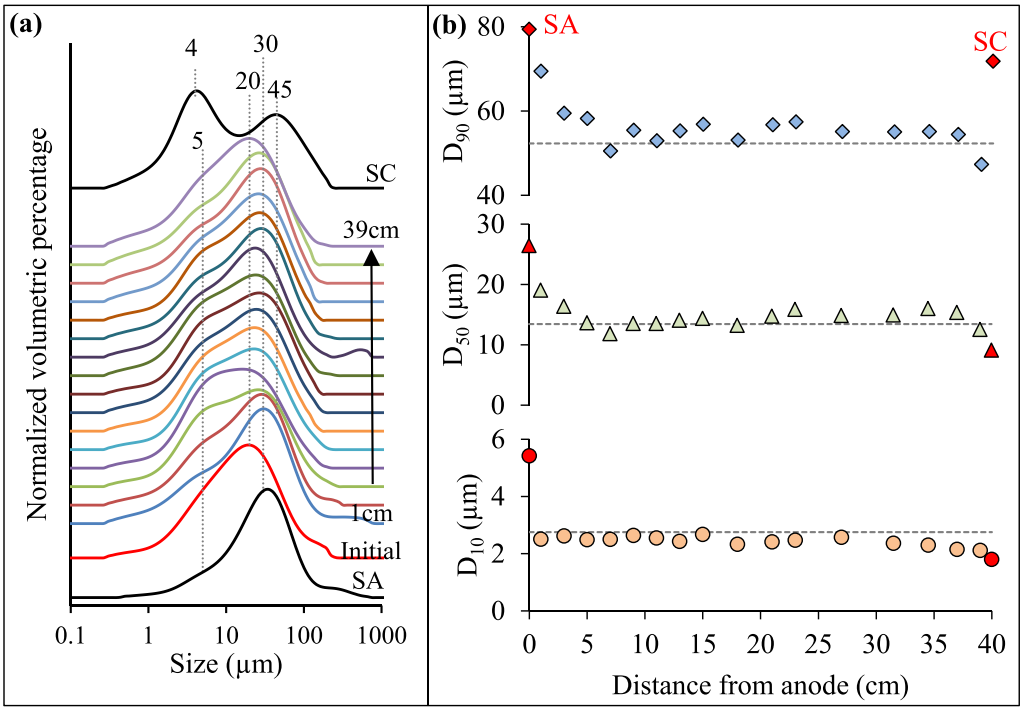

Fig. 5. Grain size distribution of the initial and treated sediments and the settled materials (SA and SC) at the end of the experiment; curves for sonicated samples are plotted. b) The percentiles (D_{10}, D_{50}, and D_{90}) of the sediments, SA, and SC as a function of distance from the anode.

Persson, 2012; Moayedi et al., 2010). It is also known that the electro-osmotic flow is mainly directed toward the cathode (e.g., Ammami et al., 2015; Wen et al., 2021; Zhou et al., 2021). Moreover, the water content reflects the texture and composition of the sediment (e.g., clay and organic contents). Finally, the water content of the combined treated sediment (53%) was significantly reduced in comparison to the initial water content (63 %).

3.4. Grain size properties

Similar to a previous study, the sediments lost their aggregation properties after EKR, as seen by the insignificance between the GSD of the sonicated and non-sonicated sediments (Kanbar et al., 2023). The treated sediments were coarser than the initial one, as mainly seen by the shift of the GSD population from 20 to 30 μm for most sediments (Fig. 5a). Furthermore, the treated sediments showed a protrusion of fine particles, as indicated by 5 μm shoulders. The GSD percentiles, D_{50} and D_{90}, showed a decreasing trend in the 0–10 cm sediments, while these percentiles were quasi-stable for the other sediments and comparable to the initial sediment. In most 10–38 cm sediments, the D_{50} and D_{90} values were slightly higher than those of the initial one, and the 38–40 cm sediment was relatively finer. Finally, the SA had relatively coarse particles when compared to the sediments and SC (Fig. 5a and b). The SC had a multi-population GSD that peaked at 4 and 45 μm, while that of SA was unimodal and peaked at 30 μm.

3.5. Mineral and organic composition

The mineral composition of the initial sediment is included in Table 1. After EKR, the carbonate mineral composition changed, namely aragonite, calcite, and dolomite. Indeed, those minerals were completely removed from the 0 – 2 and 2–4 cm sediments (insets in Fig. 6a). It is with certainty that those carbonates dissolved and were not below the detection limits since no carbonates were detected by the calcimetric method (Fig. 6b). The carbonate content then increased from the 4–6 cm sediment towards the 10–12 cm sediment and then was comparable with the initial sediment for the 12–40 cm sections. The carbonate content of the SC was ~40 % (Fig. 6b), indicating that carbonates precipitated in the cathode chamber. Indeed, among the crystalline minerals, SC contained 39 % calcite and 55 % hydrotalcite, an Mg-carbonate (Supplementary Materials 1, SM 1). As for SA, it was mainly made from graphite (95 %) caused by the degradation of the electrode material and secondly from brushite (2 %) that precipitated in the anode chamber (SM 1). It is worth noting that gypsum precipitated on top of the sediments in the anodic zone; surface samples (top ~2 – 5 mm) and foam samples (that formed on top of the sediments) towards the anode chamber contained gypsum (SM 2).

The 0–4 cm and 30–40 cm sediments had lower OM contents than the initial sediment (Fig. 6b). Due to the removal of carbonates in the 0–4 cm sediments (~30 %), it was expected that the OM content would be overestimated (since a large part of the sediment is removed, the contents, per unit mass, of the other components are relatively higher). However, this was not the case, which indicates that OM was clearly removed or degraded in the 0 – 4 cm sediments. The oxic state of the anodic sediments can chemically degrade OM more rapidly compared to the reducing conditions in the cathodic sediments (Kristensen et al., 1995; Sahrawat, 2003). The alkaline conditions in the cathodic sediments also promote OM dissolution, thus explaining lower OM contents compared to the initial sediment. The OM contents for SA and SC were 82.8 % and 30.2 %, respectively. This indicates that dissolved OM was mobilized to the chambers and precipitated, mainly in the anode chamber.

3.6. Metal(loid) and Cl behavior

The variation in elemental contents is mainly assessed through the removal, reduction, or translocation of major metals (Na, Mg, and Ca) and non-metal (Cl). The removal or reduction of salts is significant after EKR, as indicated by the reduction of Na and Cl in most sediments (Fig. 7a and b). The initial Na content was ~0.5 % and dropped to <0.05 % for most sediment sections (0 – 30 cm, Fig. 7a). However, Na accumulated in the 36–40 cm sediments and was enriched in the SC. The accumulation of Na in those sections is mainly explained by its cationic nature that causes its migration towards the cathode; the enrichment of Na in the SC is due to its precipitation in the cathode chamber, possibly through reactions with citrate (e.g., formation of tri-sodium citrate dihydrate complexes, SM 1). As for Cl, it was reduced in the sediments throughout the EKR reactor (Fig. 7b). The initial Cl content was 6.8 % and decreased to <0.05 % in the 8 – 40 cm sediments and to ~2–6 % in the 0 – 6 cm sediments. Both the SA (~16 % Cl) and SC (~11 % Cl) contained higher Cl contents compared to the initial sediment. Magnesium contents were reduced in the 0 – 20 cm sediments. A fraction of those removed Mg was transported and accumulated in the 24 – 40 cm sediments (Fig. 7c). The enrichment of Mg in the SC is thought to come

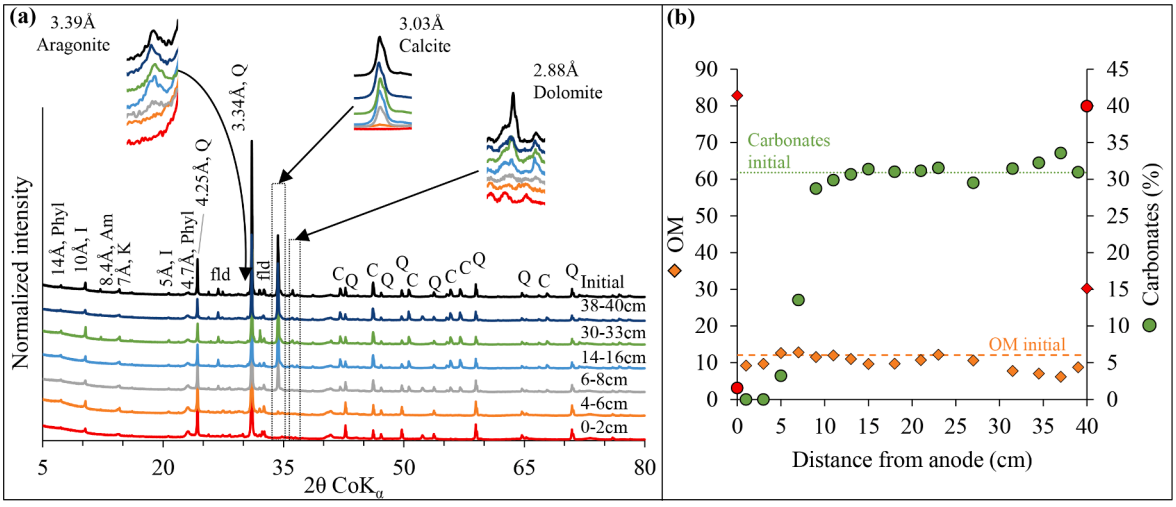

Fig. 6. Spatial variation of a) the mineral composition (XRD) for sediments after treatment; Phyl: phyllosilicates, I: illite, Am: amphibole, K: kaolinite, Q: quartz, C: calcite, and fld: feldspars; the insets highlight the variation in carbonate mineral abundances. b) Spatial variation of the carbonate and organic matter contents of sediments and settled materials (SA and SC, in red) at the end of the EKR experiment. The initial OM (dashed) and carbonate (dotted) contents are plotted for comparison purposes.

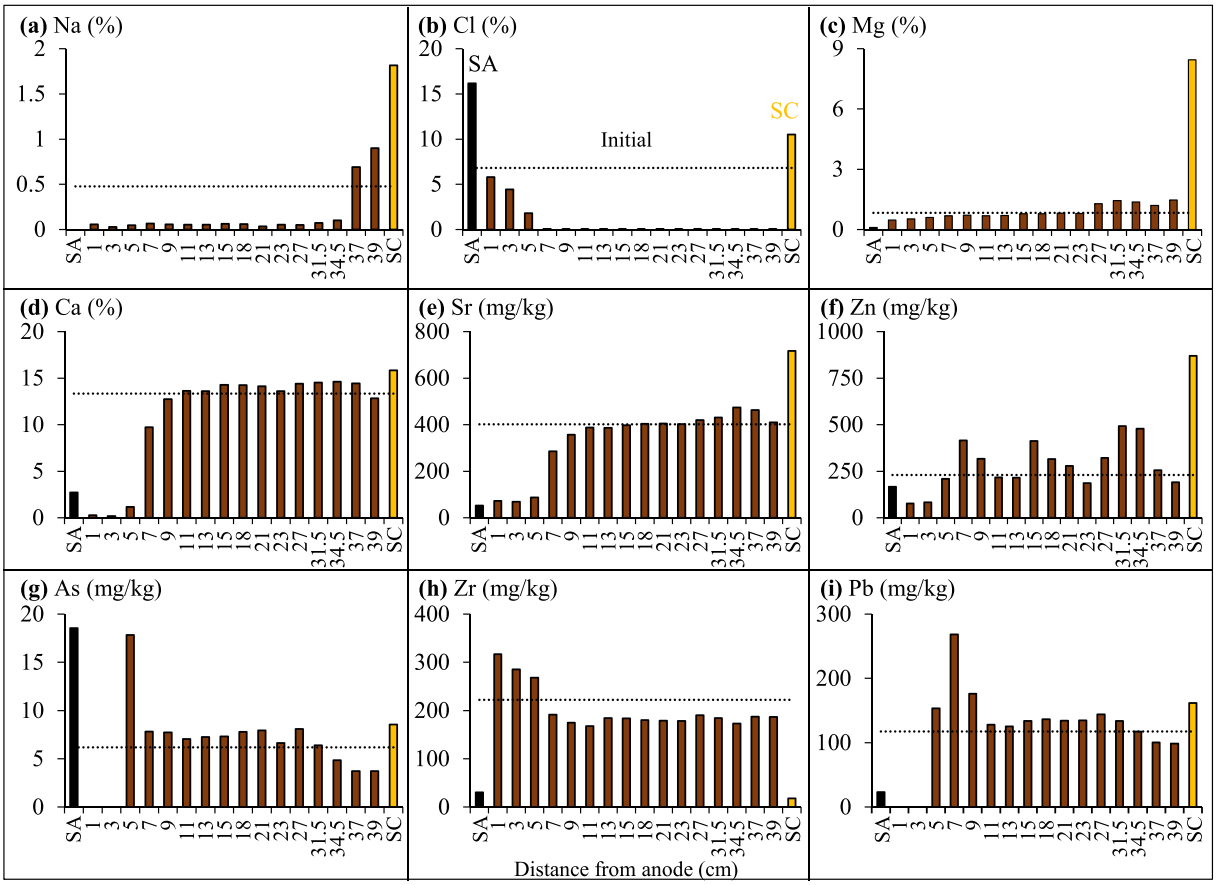

Fig. 7. The variation of a) Na (%), b) Cl (%), c) Mg (%), d) Ca (%), e) Sr (mg/kg), f) Zn (mg/kg), g) As (mg/kg), h) Zr (mg/kg), and i) Pb (mg/kg) in the sediments, SA, and SC after treatment. The dotted lines represent the initial contents.

from the precipitation of hydrotalcite or tri-magnesium di-citrate, as proven by XRD (SM 1). Only a negligible fraction of Ca remained in the 0 – 4 cm sediments after treatment (~0.2 % out of 13.3 %, Fig. 7d). However, Ca contents then became higher in the sediments farther away from the anode and reached contents similar to the initial sediment after 10 cm. The relatively high Ca content in the SC is due to carbonate precipitation (Fig. 6b), namely calcite (SM 1). Strontium followed a trend similar to Ca; however, Sr contents in the 0–16 cm sediments were lower than the initial sediment, while it was 0–10 cm for Ca. Strontium is found in carbonate minerals (Brand et al., 1998), thus both Ca and Sr cations are expected to move towards the cathode electrode after carbonate dissolution in the anodic sediments.

The distribution of the trace elements Zn, As, Zr, and Pb was peculiar. Zinc did not show a clear trend along the anode – cathode direction (Fig. 7f). The Zn contents of the 0 – 6 cm sediments were lower than the initial sediment, while other sections had higher Zn contents (e.g., 6–10, 14–20, and 30–36 cm). The SC was significantly enriched in Zn and had almost 4-fold higher Zn content compared to the initial sediment, while the SA had lower Zn contents. In a similar way to Zn, As was highly reduced, or even removed, from the 0–4 cm sediments (Fig. 7g). A big part of the removed As appeared to have accumulated in the 4–6 cm section; another part moved to the anode chamber, due to its anionic nature, where it accumulated and precipitated in the SA (~36 mg/kg). Additionally, As contents in the 33–40 cm sediments were lower than the initial sediment, while the SC was enriched in As. Zirconium contents were lower than the initial sediment for most sections, i.e., 6–40 cm (Fig. 7h). However, the reduced Zr seems to have mobilized toward the anode, as seen by an increasing trend from 6 cm toward the anode chamber. It should be noted that the relatively high Zr contents (and other elements) in the anodic zone can be overestimations due to the high carbonate loss (as explained in Section 3.5). Even though SA and SC contained some Zr, neither SA nor SC showed to preferentially sorb Zr. Regarding Pb, it was almost completely removed from the 0–4 cm sections (Fig. 7i). The Pb contents were then higher than the initial content in the 4–10 cm sections (e.g., the 6–8 cm sediment had ~2-fold the initial Pb content). The 10–30 cm sediments showed comparable Pb contents to the initial sediment, and the 36 – 40 cm sediments had relatively low Pb contents. Some of the released Pb migrated towards the cathode region and precipitated with the SC. Finally, Na, Cl, Ca, Sr, and Zr were reduced by 72 %, 90 %, 11 %, 11 %, and 11 %, respectively, and Mg, Zn, As, and Pb were mostly redistributed within the reactor. Zirconium, As, and Pb mainly accumulated in the anodic sediments, Na, Mg, Sr, and Zn were relatively high in the SC, and Cl and As were relatively high in the SA.

4. Discussion

4.1. Instant changes caused by electrokinetics

The increase in electric current and EC at the beginning of the experiment is expected due to the introduction of conductive species in the electrolyte chambers and porewater (Beyrami, 2021; Liu et al., 2023). Under a constant voltage gradient, the current increase is directly related to the decrease in resistance (Ohm's law), which is reflected by an increase in EC. The primary ions that reflect EC, and therefore current, increase are H^+ and OH^- due to their relatively high ionic conductance or mobility; the secondary ions are those that are released from the sediments due to desorption or dissolution of phases, such as carbonates (Fig. 6a and b). Indeed, H^+ and OH^- have the highest ionic conductance values (34.9 and 19.8 mS.m^2/mol, respectively), followed

by citrate (4.8 mS.m^2/mol), and then other ions, such as Ca^{2+}, Mg^{2+}, Na^+, K^+, and Cl^- (5.9, 5.3, 5.1, 7.3, and 7.6 mS.m^2/mol, respectively) (Vanysek, 1993). The EC variation caused by sedimentary processes, e.g., dissolution and precipitation, might be hidden due to the more significant H^+ and OH^- control over EC changes. In any case, the increase in current was due to an EC increase, partly from salts that are present in the estuarine sediment (e.g., Micic et al., 2001). This in turn promotes the release of metals either by substitution/replacement of metals by salt cations through competition or by the complexation of salt anions with metals (e.g., Acosta et al., 2011). However, the increase in current also depends on sediment composition; although the dissolution of carbonates and Ca release into the PW occurred in the sediments in the anodic zone (Figs. 4a and 6a and b), its effect on EC change is below that of H^+ production in the anode chamber. Furthermore, the degree and duration of EC and current increase depend on the electric parameters (e.g., the current and therefore the amount of H^+ produced) and the capability of the sediments to release conductive species (via desorption or dissolution processes). In this case, and under periodic current application, that increase occurred during the first five days (Fig. 2a). Other studies with voltage gradients between 1.33 and 2.66 V/cm also showed this initial current increase (e.g., Beyrami, 2021; Liu et al., 2023). Under a 2 V/cm gradient, the decrease in current was observed after ~48 hrs when 1 M NaCl was used, 20 hrs when 0.1 M citric acid was used, and 18 hrs when 0.5 M citric acid was used (Liu et al., 2023). In a previous study using a 0.5 V/cm gradient and running parameters similar to this study, the current only showed a decreasing trend with time (Kanbar et al., 2023). The increase in current and its duration is not directly correlated to the voltage gradient, as other factors affect this parameter, such as concentration and type of electrolyte, periodicity or intermittence of electricity, and type of medium (e.g., Ammami et al., 2013, 2015; Beyrami, 2021; Liu et al., 2023; Song et al., 2016).

4.2. *Three distinct phases explain the processes that occurred during electrokinetic remediation*

Based on the electrical and physico-chemical variations, three phases explained the EKR processes, which are grouped into days 1 – 5, 6 – 14, and 15 – 21 (Fig. 8). This grouping was mainly based on the current since it is correlated to H^+, EC, and temperature (i.e., physico-chemical parameters). Phase 1 showed the most significant variations, such as significant pH decline and increase in the anode and cathode chambers, respectively. The EC, ORP, and electric parameters also showed significant changes during those days (Figs. 2 and 3). In that phase (days 1 – 5), the evolution of pH and ORP measurements in the anode chamber were oppositely correlated to those in the cathode chamber (Fig. 8a); this correlation was only obvious in the first phase. The EC in both chambers behaved similarly in the first phase, then this correlation progressively decreased in phases 2 and 3 (Fig. 8a-c). All this information indicates that the major variations or processes that occurred in the anode and cathode chambers are dependent on the experimental conditions, such as electric parameters and the nature of the anode and cathode solutions. As such, the variation during the first five days is explained by the introduction of H^+ and OH^- caused by the oxidation and reduction of water in the anode and cathode chambers, respectively. Indeed, this is further verified by the strong and positive correlation between the EC and current in the first phase as well as the high percentage of the variance (PC1: 80 %) explained by those parameters (Fig. 8a). It should be noted that the correlation between EC and current in the third phase is due to the steady decline of these parameters.

In comparison to the first phase, the second phase (days 6 – 14) marked further variations as indicated by a change among variables' correlations on the one hand, and by a drop in variance on the other (PC1 dropped from 80 % in phase 1 to 54 % in phase 2, Fig. 8a and b). In the second phase, the physico-chemical parameters in the anode chamber were negatively linked to the electric parameters, while there was no link with those in the cathode chamber (Fig. 8b), as also indicated by pH and EC daily variations (Fig. 3). Additionally, there existed strong EC and temperature connections in the cathode chamber during all 3 phases, while this was only the case in phase 1 for the anode chamber. This correlation is mainly linked to current and subsequent temperature evolution (Kaviany, 1995). The variation in correlations between the anode and cathode chambers indicates that more processes occur in the former. Furthermore, the correlation between the parameters that were identified in phase 1 was absent in the second phase, indicating that other processes predominated. Indeed, the significant EC increase during day 8 and its unrelatedness to the current can be explained by the dissolution of phases, probably carbonates (Fig. 6a and b).

The third phase (days 15 – 21) marked further variations in the system. This variation might be due to changes in the porewater composition. One sign is the reduction of EC and current (Fig. 2a and 3c), which can further be linked to less available ionic species in the PW and electrolyte chambers, subsequently suggesting precipitation. Indeed, calcium released from carbonate dissolution formed gypsum on the surface of the sediment due to the relatively high temperatures (SM 2). Gypsum precipitates at a wide range of pH, although low pHs are more favorable (~ 2 – 3), and at relatively high temperatures (40 – 60 °C) (Van Driessche et al., 2019; Xu et al., 2019), such as the case of the sediments in the anodic zone. However, this does not indicate that carbonate dissolution and mineral precipitation (e.g., gypsum) did not happen in the first two phases. In general, the variations occurring in this phase are highly linked to variations in the current and subsequently variations in EC and T (63 % of variance, Fig. 8c).

Finally, the different phases and possible processes that occur in sediment/porewater (or other matrices such as soil) can be monitored by

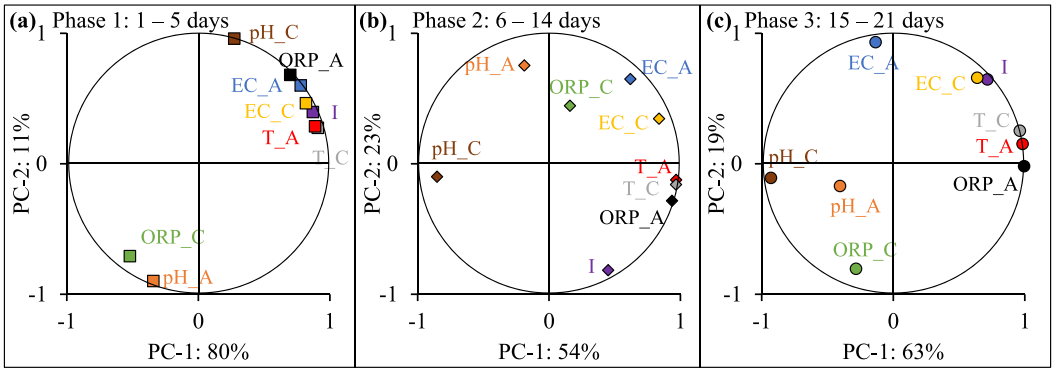

Fig. 8. The correlation between pH, EC, ORP, I, and T in the anode and cathode chambers (noted "A" and "C", respectively), as represented by principal component analyses (PCA), during the three phases (days 1 – 5, 6 – 14, and 15 – 21).

such parameters and approaches. Indeed, continuous monitoring has proven significant in controlling EKR (Betremieux and Mamindy-Pajany, 2022 e.g., Millán et al., 2020). Such info can be used to avoid reaching unwanted results (e.g., carbonate dissolution); carbonates are important components in soils that maintain a high buffering capacity. This approach can also be used to determine the end of the treatment period since those parameters reflect EKR efficacy (Ammami et al., 2015; Han et al., 2021; Mohammad et al., 2022). In general, a few days up to three weeks have been proven to sufficiently remediate matrices (e.g., Hahladakis et al., 2016; Li et al., 2021; Ortiz-Soto et al., 2023). In our case, the experiment could have been terminated at the end of phase 2, since it showed a significant reduction in ionic species, reflecting decreased metal desorption from the sediment. Halting the experiment after phase 2 might have also preserved carbonates, as the carbonate dissolution rate seemed to have increased during the third phase.

4.3. Electrokinetic remediation changed bulk sedimentary characteristics

It is clear that the sedimentary characteristics changed after EKR, which is expected due to the application of a DC current and subsequent alterations caused by producing H^+ and OH^- (i.e., changing pH), increasing temperature, and liberating ionic species from the sediment (e.g., surface-bound or carbonate dissolution). Indeed, all those changes affect the remediation efficiency as they control elemental behavior (Carrillo-González et al., 2006; Du Laing et al., 2009; Han et al., 2021; Wen et al., 2021). At the bulk scale, the physical properties (i.e., GSD, Fig. 5) and water content (Fig. 4d) of the sediments varied along the anode – cathode direction. These variations are mainly associated with sediment composition, such as organic matter and clay contents, which are positively linked to water content (e.g., Husein Malkawi et al., 1999; Menounos, 1997). Although the GSD of the sediments shifted towards coarser sizes after EKR, it is unlikely that the physical properties of the clay minerals changed. Rather, it is the dissolution of carbonates and particulate organic matter in the anodic and cathodic sediments, respectively, as well as precipitation of other phases that changed the GSD; gypsum, which precipitated on the sediment surface and in the anodic zone, is one of these phases (SM 2). The alkaline conditions of the cathodic sediments are able to dissolve organic matter that subsequently mobilizes towards the anode (Maqbool and Jiang, 2023). In our case, organic matter enrichment was not detected in the anodic sediments (Fig. 6b). The absence of that direct link in this study might be due to other dissolution/precipitation processes that occurred during EKR that change the particulate mass (i.e., ~31 % carbonates in the anodic zone) and therefore OM contents. However, it is possible that the dissolved OM migrated towards the anode chamber where it precipitated, as suggested by the highly OM-enriched SA (~83 %, Fig. 6b).

The major cations, such as Na and Mg, are surrounded by the partially negatively-charged oxygen atoms of water molecules (e.g., Kiriukhin and Collins, 2002; Stangret and Gampe, 2002). These hydration spheres, including cations, are then translocated toward the cathode. Oppositely, anionic species, such as Cl and As, are surrounded by the partially positively-charged hydrogen atoms of water molecules and are mobilized towards the anode. As a result of both processes, water translocates within the sediments mainly towards the electrodes. Indeed, the 10–30 cm sediments showed relatively low water contents (Fig. 4d). In that regard, Ouhadi et al. (2010) showed that water mobilized towards the cathode due to the formation of hydration spheres around dissolved cationic species. In our case, and due to the heterogeneous composition of the estuarine sediments, water molecules flowed towards both electrodes; net positive hydration spheres migrated towards the cathode while negative ones migrated towards the anode.

4.4. Mobility of metal(loid)s and Cl in sediments, accumulation, and precipitation

The H^+ and other cations present in the anodic sediments, e.g., due to carbonate and salt dissolution or desorption, compete with surface-bound metals (e.g., Du Laing et al., 2009). The main EC increase was seen in the first 8 days (Fig. 3a), suggesting that the highest metal release and mobility occurred then. The main processes governed by the release of H^+ and OH^- are discussed elsewhere (Kanbar et al., 2023). Two main processes account for what occurred in the sediments (Fig. 9). The first component explains 62% of the variance and is strongly linked to carbonate content (i.e., carbonate dissolution). The second component explains 18% of the variance and is linked to cations that are mainly released as a result of salt dissolution (release of Na and Mg), which further compete with other metals and cause their release (e.g., Du Laing et al., 2009). The acidic conditions caused by the generation of H^+ in the anode chamber and its mobilization towards the cathode promotes carbonate dissolution, which in turn releases associated metals, such as Sr (Brand et al., 1998). Zirconium, and to a lesser extent Zn and Pb, were linked to the pH conditions of the sediment; the former is negatively linked while the others are positively linked. The release of major cations, such as Na and Mg, as well as trace metal(loid)s (e.g., As, Pb, and Zr) were also pH-dependent. Furthermore, such metals, in addition to H^+, compete with surface metals and thus causing their release (Carrillo-González et al., 2006). Although the generation of H^+ and OH^- explain EC variation, the remaining Cl contents in the sediments, and therefore the released/mobilized Cl, also explain EC variation (Fig. 9). Interestingly, the elements that were released from the sediment and migrated towards the anodic (e.g., Cl and As) and cathodic (e.g., Na, Mg, Zn, and Sr) zones were part of the elements that later precipitated in the SA and SC, respectively. Such materials promote the accumulation of unwanted materials present in sediments and make them less labile. The SA and SC represented element-specific sorption media. The physico-chemical properties of SA and the anodic sediment as well as SC and the cathodic sediment were similar (Fig. 4). On the other hand, the physical (GSD), mineral, organic, and chemical contents were quite different (Figs. 5, 6b, SM 1, and 7). The notion of specific sorption or accumulation of elements/metals using natural or anthropogenic materials is useful not only to remediate sediments (or other matrices), but also to facilitate the reuse of such metal-rich media.

Although certain elements were removed from the sediments and precipitated in the chambers (SA and SC, Fig. 7), a big part of them were merely translocated in the reactor. Sodium and Cl were removed from most sediments except the cathodic and anodic zones, respectively. Other elements such as Zr and Pb were removed from specific sections.

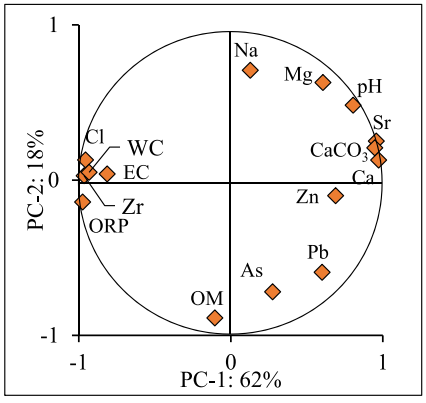

Fig. 9. Principal component analysis (PCA) matrix for the elemental contents (As, Ca, Cl, Mg, Na, Pb, Sr, Zn, and Zr), carbonates ($CaCO_3$), organic matter (OM), water content (WC), and physico-chemical characteristics (pH, ORP, and EC) of the sediments after treatment.

The variation in removal efficiency and only the translocation of chemicals is dependent on factors including anolyte and catholyte composition, DC voltage gradient, type of matrix, and metal species. Therefore, concentrating metals in specific sections can be anticipated (e.g., Benamar et al., 2019; Ortiz-Soto et al., 2023). Anyway, the EK treatment narrowed the enrichment of some elements in certain zones. As a result, and for efficient implementation of the treated material, selected sections within acceptable limits can be reused. For example, 4–8 cm sediments are highly enriched in As and Pb and thus can be discarded for further use (depending on intended use); alternatively, these elemental-rich sections can be used to farm valuable elements (e.g., Van der Ent et al., 2018). The translocation of some metals can be linked to the migration of hydration spheres (see Section 4.3). Indeed, the migration of hydration spheres, containing Na and Mg, toward the cathode was evidenced by the accumulation of these metals in the cathodic zone as well as in the SC (Fig. 7a and c). The same applies to Cl and As, however, these elements moved toward the anodic zone and further accumulated in the SA (Fig. 7b). The successful removal of Na and Cl largely comes from the dissolution of salts. Additionally, the great reduction in Na and Cl contents explains the significant drop in EC after treatment (Fig. 4b).

5. Conclusion

Estuarine sediments were treated using electrokinetics and the variation and evolution of physico-chemical, physical, mineral, organic, and elemental parameters were followed. Most variations occurred during the first five days of treatment, as indicated by the current evolution, which in turn reflects the ionic species within the reactor. The later variations were linked to the evolution of the acidic front, further dissolution of carbonates, consequent elemental desorption and translocation, and finally the precipitation of unique phases on the sediment surface and in the electrolyte chambers. The precipitated materials accumulated Cl and As in the anode chamber and Na, Mg, Cl, Sr, Pb, and Zn in the cathode chamber. The overall electric conductivity of the treated sediment was highly reduced as a result of salt and Cl removal (~90 %). Furthermore, the acidic conditions in the anodic zone dissolved carbonates. Consequently, Ca, As, and Pb were almost entirely removed and Zn was reduced by ~65 % from the anodic sediments. Oppositely, Zr contents were reduced in all the sections except in the anodic sediments; indeed, Zr was removed from the 6–40 cm sediments and accumulated in the 0–6 cm region. The treated sediment overall had significantly lower metal and salt contents and was used for agricultural purposes (ReCon Soil project). Finally, understanding those processes and their connection to sediment components can be used to assess the effectiveness of the EKR technique and also to prevent undesirable outcomes like carbonate dissolution, depending on the intended use of the sediment.

Funding

This work was funded by the European Regional Development Fund (ERDF), Interreg France (Channel Manche) England, ReCon Soil project. The funding source had no role in the study design, in the collection, analysis, and interpretation of data, in the writing of the report, and in the decision to submit the article for publication.

CRediT authorship contribution statement

Hussein J. Kanbar: Writing – review & editing, Writing – original draft, Visualization, Methodology, Investigation, Formal analysis, Data curation, Conceptualization. **Mohamed-Tahar Ammami:** Writing – review & editing, Supervision, Resources, Methodology, Funding acquisition, Conceptualization. **Ahmed Benamar:** Writing – review & editing, Supervision, Resources, Methodology, Funding acquisition, Conceptualization.

Declaration of competing interest

The authors declare that they have no known competing financial interests or personal relationships that could have appeared to influence the work reported in this paper.

Data availability

Data will be made available on request.

Acknowledgements

The authors acknowledge Dr. Benoît Duchemin (LOMC, Le Havre University) for valuable help in running XRD. We are most grateful to PLATIN' (Plateau d'Isotopie de Normandie) core facility for all element and isotope analysis used in this study; we particularly thank Dr. Fanny Leroy for her help in reporting the precision of elemental quantification using XRF.

Supplementary materials

Supplementary material associated with this article can be found, in the online version, at doi:10.1016/j.envc.2024.100880.

References

Acar, Y.B., Alshawabkeh, A.N., 1993. Principles of electrokinetic remediation. Environ. Sci. Technol. 27, 2638–2647. https://doi.org/10.1021/es00049a002.

Acosta, J.A., Jansen, B., Kalbitz, K., Faz, A., Martínez-Martínez, S., 2011. Salinity increases mobility of heavy metals in soils. Chemosphere 85, 1318–1324. https://doi.org/10.1016/j.chemosphere.2011.07.046.

Ammami, M., Benamar, A., Wang, H., Bailleul, C., Legras, M., Le Derf, F., Portet-Koltalo, F., 2013. Simultaneous electrokinetic removal of polycyclic aromatic hydrocarbons and metals from a sediment using mixed enhancing agents. Int. J. Environ. Sci. Technol. 11, 1801–1816. https://doi.org/10.1007/s13762-013-0395-9.

Ammami, M., Song, Y., Benamar, A., Portet-Koltalo, F., Wang, H., 2020. Electro-dewatering of dredged sediments by combined effects of mechanical and electrical processes: influence of operating conditions. Electrochim. Acta 353, 136462. https://doi.org/10.1016/j.electacta.2020.136462.

Ammami, M.T., Benamar, A., Portet-Koltalo, F., 2022. Enhanced electroremediation of metals from dredged marine sediment under periodic voltage using EDDS and citric acid. J. Mar. Sci. Eng. 10, 553. https://doi.org/10.3390/jmse10040553.

Ammami, M.T., Portet-Koltalo, F., Benamar, A., Duclairoir-Poc, C., Wang, H., Le Derf, F., 2015. Application of biosurfactants and periodic voltage gradient for enhanced electrokinetic remediation of metals and PAHs in dredged marine sediments. Chemosphere 125, 1–8. https://doi.org/10.1016/j.chemosphere.2014.12.087.

Apitz, S.E., 2010. Waste or resource? Classifying and scoring dredged material management strategies in terms of the waste hierarchy. J. Soils Sediments 10, 1657–1668. https://doi.org/10.1007/s11368-010-0300-9.

Benamar, A., Ammami, M.-T., Kanbar, H., 2024. Managing dredged sediments: evolution of land deposit and assessment of benefit reuse. In: Attila, Ç., Barbieri, M., Khan, M. F., Ugulu, I., Turan, V., Knight, J., Rodrigo-Comino, J., Chenchouni, H., Radwan, A. E., Kallel, A., Panagoulia, D., Candeias, C., Biswas, A., Chaminé, H.I., Gentilucci, M., Bezzeghoud, M., Ergüler, Z.A. (Eds.), Recent Research on Environmental Earth Sciences, Geomorphology, Soil Science and Paleoenvironments. Proceedings of the 2nd MedGU, Marrakesh 2022. Morocco. Springer Cham, Marrakesh, p. 294.

Benamar, A., Tian, Y., Portet-Koltalo, F., Ammami, M., Giusti-Petrucciani, N., Song, Y., Boulangé-Lecomte, C., 2019. Enhanced electrokinetic remediation of multi-contaminated dredged sediments and induced effect on their toxicity. Chemosphere 228, 744–755. https://doi.org/10.1016/j.chemosphere.2019.04.063.

Betremieux, M., Mamindy-Pajany, Y., 2022. Investigation of a biosurfactant-enhanced electrokinetic method and its effect on the potentially toxic trace elements in waterways sediments. Environ. Technol. 43, 3870–3887. https://doi.org/10.1080/09593330.2021.1936202.

Beyrami, H., 2021. Effect of different treatments on electrokinetic remediation of Zn, Pb and Cd from a contaminated calcareous soil. Chin. J. Chem. Eng. 38, 255–265. https://doi.org/10.1016/j.cjche.2020.09.011.

Bose, B.P., Dhar, M., 2022. Dredged sediments are one of the valuable resources : a review. Int. J. Earth Sci. Knowl. Appl. 4, 324–331.

Brand, U., Morrison, J.O., Campbell, I.T., 1998. Strontium in sedimentary rocks. In: Marshall, C.P., Fairbridge, R.W. (Eds.), Encyclopedia of Geochemistry. Kluwer Academic Publishers, Dordrecht, pp. 600–603. https://doi.org/10.1007/1-4020-4496-8_301.

Cameselle, C., Chirakkara, R.A., Reddy, K.R., 2013. Electrokinetic-enhanced phytoremediation of soils: status and opportunities. Chemosphere 93, 626–636. https://doi.org/10.1016/j.chemosphere.2013.06.029.

Caporale, A.G., Violante, A., 2016. Chemical processes affecting the mobility of heavy metals and metalloids in soil environments. Curr. Pollut. Reports 2, 15–27. https://doi.org/10.1007/s40726-015-0024-y.

Carrillo-González, R., Šimůnek, J., Sauvé, S., Adriano, D.C., 2006. Mechanisms and pathways of trace element mobility in soils. In: Sparks, D.L. (Ed.), Advances in Agronomy. Elsevier, pp. 111–178. https://doi.org/10.1016/S0065-2113(06)91003-7.

Chen, X., Kumari, D., Cao, C.J., Plaza, G., Achal, V., 2020. A review on remediation technologies for nickel-contaminated soil. Hum. Ecol. Risk Assess. 26, 571–585. https://doi.org/10.1080/10807039.2018.1539639.

Churchman, G.J., Singh, M., Schapel, A., Sarkar, B., Bolan, N., 2020. Clay minerals as the key to the sequestration of carbon in soils. Clays. Clay. Miner. 68, 135–143. https://doi.org/10.1007/s42860-020-00071-z.

Döbelin, N., 2021. Profex: open source XRD and Rietveld refinement [WWW Document]. URL. https://www.profex-xrd.org/(accessed 3.26.21).

Doebelin, N., Kleeberg, R., 2015. Profex: a graphical user interface for the Rietveld refinement program BGMN. J. Appl. Crystallogr. 48, 1573–1580. https://doi.org/10.1107/S1600576715014685.

Du Laing, G., De Vos, R., Vandecasteele, B., Lesage, E., Tack, F.M.G., Verloo, M.G., 2008. Effect of salinity on heavy metal mobility and availability in intertidal sediments of the Scheldt estuary. Estuar. Coast. Shelf Sci. 77, 589–602. https://doi.org/10.1016/j.ecss.2007.10.017.

Du Laing, G., Rinklebe, J., Vandecasteele, B., Meers, E., Tack, F.M.G., 2009. Trace metal behaviour in estuarine and riverine floodplain soils and sediments: a review. Sci. Total Environ. 407, 3972–3985. https://doi.org/10.1016/j.scitotenv.2008.07.025.

Du Laing, G., Vandecasteele, B., De Grauwe, P., Moors, W., Lesage, E., Meers, E., Tack, F. M.G., Verloo, M.G., Grauwe, P., De, 2007. Factors affecting metal concentrations in the upper sediment layer of intertidal reedbeds along the river Scheldt. J. Environ. Monit. 9, 449–455. https://doi.org/10.1039/b618772b.

Elzinga, E.J., Reeder, R.J., 2002. X-ray absorption spectroscopy study of Cu^{2+} and Zn^{2+} adsorption complexes at the calcite surface: implications for site-specific metal incorporation preferences during calcite crystal growth. Geochim. Cosmochim. Acta 66, 3943–3954. https://doi.org/10.1016/S0016-7037(02)00971-7.

Elzinga, E.J., Rouff, A.A., Reeder, R.J., 2006. The long-term fate of Cu^{2+}, Zn^{2+}, and Pb^{2+} adsorption complexes at the calcite surface: an X-ray absorption spectroscopy study. Geochim. Cosmochim. Acta 70, 2715–2725. https://doi.org/10.1016/j.gca.2006.02.026.

EU, 2019. Regulation (EU) 2019/1009 of the European Parliament and of the Council of 5 June 2019, laying down rules on the making available on the market of EU fertilising products and amending. Off. J. Eur. Union L170, 1–114.

EU, 2008a. Directive 2008/98/EC of the European Parliament and of the Council of 19 November 2008 on waste and repealing certain directives. Off. J. Eur. Union L312, 3–30.

EU, 2008b. Directive 2008/58/EC of the European Parliament and of the Council of 17 June 2008 establishing a framework for community action in the field of marine environmental policy (Marine Strategy Framework Directive). Off. J. Eur. Community L164, 19–40.

EU, 2000. Directive 2000/60/EC of the European Parliament and of the Council of 23 October 2000 establishing a framework for Community action in the field of water policy. Off. J. Eur. Communities L327, 1–73.

Ferrans, L., Schmieder, F., Mugwira, R., Marques, M., Hogland, W., 2022. Dredged sediments as a plant-growing substrate: estimation of health risk index. Sci. Total Environ. 846, 157463 https://doi.org/10.1016/j.scitotenv.2022.157463.

Gorji, T., Yildirim, A., Hamzehpour, N., Tanik, A., Sertel, E., 2020. Soil salinity analysis of Urmia Lake Basin using Landsat-8 OLI and Sentinel-2A based spectral indices and electrical conductivity measurements. Ecol. Indic. 112, 106173 https://doi.org/10.1016/j.ecolind.2020.106173.

Govindaraju, K., 1989. Compilation of working values and sample description for 272 geostandards. Geostand. Newsl. 13, 1–113. https://doi.org/10.1111/j.1751-908X.1989.tb00476.x.

Grabowski, R.C., Droppo, I.G., Wharton, G., 2011. Erodibility of cohesive sediment: the importance of sediment properties. Earth-Sci. Rev. 105, 101–120. https://doi.org/10.1016/j.earscirev.2011.01.008.

Hahladakis, J.N., Latsos, A., Gidarakos, E., 2016. Performance of electroremediation in real contaminated sediments using a big cell, periodic voltage and innovative surfactants. J. Hazard. Mater. 320, 376–385. https://doi.org/10.1016/j.jhazmat.2016.08.003.

Hahn, J., Bui, T., Kessler, M., Weber, C.J., Beier, T., Mildenberger, A., Traub, M., Opp, C., 2022. Catchment soil properties affect metal(loid) enrichment in reservoir sediments of German low mountain regions. Appl. Sci. 12 https://doi.org/10.3390/app12052277.

Han, D., Wu, X., Li, R., Tang, X., Xiao, S., Scholz, M., 2021. Critical review of electrokinetic remediation of contaminated soils and sediments: mechanisms, performances and technologies. Water. Air. Soil Pollut. 232, 335. https://doi.org/10.1007/s11270-021-05182-4.

Heiri, O., Lotter, A.F., Lemcke, G., 2001. Loss on ignition as a method for estimating organic and carbonate content in sediments: reproducibility and comparability of results. J. Paleolimnol. 25, 101–110. https://doi.org/10.1023/A:1008119611481.

Husein Malkawi, A.I., Alawneh, A.S., Abu-Safaqah, O.T., 1999. Effects of organic matter on the physical and the physicochemical properties of an illitic soil. Appl. Clay Sci. 14, 257–278. https://doi.org/10.1016/S0169-1317(99)00003-4.

Interreg ReCon Soil, 2022. Reconstructed Soils from Waste. ReCon Soil [WWW Document], France (Channel Manche) England. URL. https://www.channelmanche.com/en/projects/approved-projects/reconstructed-soils-from-waste/ (accessed 11.21.22).

ISO 10693, 1995. ISO 10693 [WWW Document]. URL. https://www.iso.org/standard/18781.html.

Kanbar, H.J., Zein-Eddin, A., Ammami, M.-T., Benamar, A., 2023. Electrokinetic remediation of estuarine sediments using a large reactor: spatial variation of physicochemical, mineral, and chemical properties. Environ. Sci. Pollut. Res. 30, 117688–117705. https://doi.org/10.1007/s11356-023-30271-8.

Kaviany, M., 1995. Principles of Heat Transfer in Porous Media. 2nd ed, Mechanical Engineering Series. Springer New York, New York, NY. https://doi.org/10.1007/978-1-4612-4254-3.

Kiani, M., Raave, H., Simojoki, A., Tammeorg, O., Tammeorg, P., 2021. Recycling lake sediment to agriculture: effects on plant growth, nutrient availability, and leaching. Sci. Total Environ. 753, 141984 https://doi.org/10.1016/j.scitotenv.2020.141984.

Kim, W.S., Park, G.Y., Kim, D.H., Jung, H.B., Ko, S.H., Baek, K., 2012. In situ field scale electrokinetic remediation of multi-metals contaminated paddy soil: influence of electrode configuration. Electrochim. Acta 86, 89–95. https://doi.org/10.1016/j.electacta.2012.02.078.

Kiriukhin, M.Y., Collins, K.D., 2002. Dynamic hydration numbers for biologically important ions. Biophys. Chem. 99, 155–168. https://doi.org/10.1016/S0301-4622(02)00153-9.

Kristensen, E., Ahmed, S.I., Devol, A.H., 1995. Aerobic and anaerobic decomposition of organic matter in marine sediment: which is fastest? Limnol. Oceanogr. 40, 1430–1437. https://doi.org/10.4319/lo.1995.40.8.1430.

Li, J., Chen, L., Zhang, Q., Wu, L., Zhang, J., Larson, S.L., Ballard, J.H., Ma, Y., Su, Y., Han, F.X., 2021. Coupling electrokinetics and phytoremediation to remove uranium from contaminated soil: a laboratory pilot-scale study. ACS Earth Sp. Chem. acsearthspacechem.1c00286. https://doi.org/10.1021/acsearthspacechem.1c00286.

Liu, X., Xu, L., Zhuang, Y., 2023. Effect of electrolyte, potential gradient and treatment time on remediation of hexavalent chromium contaminated soil by electrokinetic remediation and adsorption. Environ. Earth Sci. 82, 40. https://doi.org/10.1007/s12665-022-10673-6.

Lynch, S., Batty, L., Byrne, P., 2014. Environmental risk of metal mining contaminated river bank sediment at redox-transitional zones. Minerals 4, 52–73. https://doi.org/10.3390/min4010052.

Macci, C., Vannucchi, F., Doni, S., Peruzzi, E., Lucchetti, S., Castellani, M., Masciandaro, G., 2022. Recovery and environmental recycling of sediments: the experience of CNR-IRET Pisa. J. Soils Sediments 22, 2865–2872. https://doi.org/10.1007/s11368-022-03162-7.

Mähler, J., Persson, I., 2012. A study of the hydration of the alkali metal ions in aqueous solution. Inorg. Chem. 51, 425–438. https://doi.org/10.1021/ic2018693.

Maqbool, T., Jiang, D., 2023. Electrokinetic remediation leads to translocation of dissolved organic matter/nutrients and oxidation of aromatics and polysaccharides. Sci. Total Environ. 162703. https://doi.org/10.1016/j.scitotenv.2023.162703.

Menounos, B., 1997. The water content of lake sediments and its relationship to other physical parameters: an alpine case study. Holocene 7, 207–212. https://doi.org/10.1177/095968369700700208.

Mesrar, L., Benamar, A., Duchemin, B., Brasselet, S., Bourdin, F., Jabrane, R., 2021. Engineering properties of dredged sediments as a raw resource for fired bricks. Bull. Eng. Geol. Environ. 80, 2643–2658. https://doi.org/10.1007/s10064-020-02068-3.

Micic, S., Shang, J.Q., Lo, K.Y., Lee, Y.N., Lee, S.W., 2001. Electrokinetic strengthening of a marine sediment using intermittent current. Can. Geotech. J. 38, 287–302. https://doi.org/10.1139/cgj-38-2-287.

Micó, C., Recatalá, L., Peris, M., Sánchez, J., 2006. Assessing heavy metal sources in agricultural soils of an European Mediterranean area by multivariate analysis. Chemosphere 65, 863–872. https://doi.org/10.1016/j.chemosphere.2006.03.016.

Millán, M., Bucio-Rodríguez, P.Y., Lobato, J., Fernández-Marchante, C.M., Roa-Morales, G., Barrera-Díaz, C., Rodrigo, M.A., 2020. Strategies for powering electrokinetic soil remediation: a way to optimize performance of the environmental technology. J. Environ. Manage. 267 https://doi.org/10.1016/j.jenvman.2020.110665.

Moayedi, H., Huat, B.B.K., Ali, T.A.M., Moghaddam, S.A., Ghazvinei, P.T., 2010. Electrokinetic injection in highly organic soil — a review. Electron. J. Geotech. Eng. 1593–1598.

Mohammad, N., Moghal, A.A.B., Rasheed, R.M., Almajed, A., 2022. Critical review on the efficacy of electrokinetic techniques in geotechnical and geoenvironmental applications. Arab. J. Geosci. 15 https://doi.org/10.1007/s12517-022-10037-1.

Ortiz-Soto, R., Leal, D., Gutierrez, C., Aracena, A., León, M., Lazo, A., Lazo, P., Ottosen, L., Hansen, H., 2023. Incidence of electric field and sulfuric acid concentration in electrokinetic remediation of Cobalt, Copper, and Nickel in fresh copper mine tailings. Processes 11, 108. https://doi.org/10.3390/pr11010108.

Ouhadi, V.R., Yong, R.N., Shariatmadari, N., Saeidijam, S., Goodarzi, A.R., Safari-Zanjani, M., 2010. Impact of carbonate on the efficiency of heavy metal removal from kaolinite soil by the electrokinetic soil remediation method. J. Hazard. Mater. 173, 87–94. https://doi.org/10.1016/j.jhazmat.2009.08.052.

Post, J.E., Bish, D.L., 1989. Rietveld refinement of crystal structures using powder X-ray diffraction data. In: Bish, David, L, Post, J.L. (Eds.), Modern Powder Diffraction. The mineralogical society of America, Washington, pp. 277–308.

Renella, G., 2021. Recycling and reuse of sediments in agriculture: where is the problem? Sustain 13, 1–12. https://doi.org/10.3390/su13041648.

Sahrawat, K.L., 2003. Organic matter accumulation in submerged soils. Advances in Agronomy. Elsevier, pp. 169–201. https://doi.org/10.1016/S0065-2113(03)81004-0.

SARM, 2015. Certificate of Analysis: Be-N Reference Material, Basalte [WWW Document]. SARM - Serv. d'Analyses des Roches des Minéraux CRPG. URL. https://sarm.cnrs.fr/wp-content/uploads/2022/04/BE-N-v_eng.pdf (accessed 2.11.24).

SedNet, 2004. Contaminated Sediments in European River Basins [WWW Document]. Eur. Sediment Res. Netw. URL www.SedNet.org (accessed 5.7.23).
Selvi, A., Rajasekar, A., Theerthagiri, J., Ananthaselvam, A., Sathishkumar, K., Madhavan, J., Rahman, P.K.S.M., 2019. Integrated remediation processes toward heavy metal removal/recovery from various environments-a review. Front. Environ. Sci. 7 https://doi.org/10.3389/fenvs.2019.00066.
Song, Y., Ammami, M., Benamar, A., Mezazigh, S., Wang, H., 2016. Effect of EDTA, EDDS, NTA and citric acid on electrokinetic remediation of As, Cd, Cr, Cu, Ni, Pb and Zn contaminated dredged marine sediment. Environ. Sci. Pollut. Res. 23, 10577–10586. https://doi.org/10.1007/s11356-015-5966-5.
Sordes, F., Pellequer, E., Sahli, S., Sarzynski, T., Denes, M., Techer, I., 2023. Phytoremediation of chloride from marine dredged sediments: a new model based on a natural vegetation recolonization. J. Environ. Manage. 344, 118508 https://doi.org/10.1016/j.jenvman.2023.118508.
Stangret, J., Gampe, T., 2002. Ionic hydration behavior derived from infrared spectra in HDO. J. Phys. Chem. A 106, 5393–5402. https://doi.org/10.1021/jp014063v.
Tian, F., Hou, M., Qiu, Y., Zhang, T., Yuan, Y., 2020. Salinity stress effects on transpiration and plant growth under different salinity soil levels based on thermal infrared remote (TIR) technique. Geoderma 357, 113961. https://doi.org/10.1016/j.geoderma.2019.113961.
Vácha, R., Čechmánková, J., Skála, J., Hofman, J., Čermák, P., Sáňka, M., Váchová, T., 2011. Use of dredged sediments on agricultural soils from viewpoint of potentially toxic substances. Plant Soil Environ. 57, 388–395. https://doi.org/10.17221/105/2011-pse.
Van der Ent, A., Echevarria, G., Baker, A.J.M., Morel, J.L., 2018. Agromining: farming for metals. Extracting Unconventional Resources Using Plants, 2nd ed. Springer Cham. https://doi.org/10.1007/978-3-319-61899-9.
Van Driessche, A.E.S., Stawski, T.M., Kellermeier, M., 2019. Calcium sulfate precipitation pathways in natural and engineered environments. Chem. Geol. 530, 119274 https://doi.org/10.1016/j.chemgeo.2019.119274.
Vanysek, P., 1993. Ionic conductivity and diffusion at infinite dilution. In: Lide, D.R. (Ed.), CRC Handbook of Chemistry and Physics. CRC press, pp. 5–77.
Vicente, M.C., Trevisan, C.L., Carvalho, A.C.B., Machado, W.T., Wasserman, J.C., 2022. A method to reproduce pH and Eh environmental changes due to sediment resuspension. MethodsX. 9, 101751 https://doi.org/10.1016/j.mex.2022.101751.
Wen, D., Fu, R., Li, Q., 2021. Removal of inorganic contaminants in soil by electrokinetic remediation technologies: a review. J. Hazard. Mater. 401, 123345 https://doi.org/10.1016/j.jhazmat.2020.123345.
Xu, Y., Liao, Y., Lin, Z., Lin, Jiang, Li, Q., Lin, Jiuyang, Jin, Z., 2019. Precipitation of calcium sulfate dihydrate in the presence of fulvic acid and magnesium ion. Chem. Eng. J. 361, 1078–1088. https://doi.org/10.1016/j.cej.2019.01.003.
Xue, Z., Tang, X., Yang, Q., 2017. Influence of voltage and temperature on electro-osmosis experiments applied on marine clay. Appl. Clay Sci. 141, 13–22. https://doi.org/10.1016/j.clay.2017.01.033.
Zhang, H., Luo, Y., Makino, T., Wu, L., Nanzyo, M., 2013. The heavy metal partition in size-fractions of the fine particles in agricultural soils contaminated by waste water and smelter dust. J. Hazard. Mater. 248–249, 303–312. https://doi.org/10.1016/j.jhazmat.2013.01.019.
Zhao, M., Ma, D., Wang, Q., Wang, Y., Sun, X., 2022. Electrokinetic remediation of Cd-contaminated soil using low voltage gradients coupled with array adsorption zone and polarity exchange. Process Saf. Environ. Prot. 157, 81–91. https://doi.org/10.1016/j.psep.2021.11.001.
Zhou, H., Liu, Z., Li, X., Xu, J., 2021. Remediation of lead (II)-contaminated soil using electrokinetics assisted by permeable reactive barrier with different filling materials. J. Hazard. Mater. 408, 124885 https://doi.org/10.1016/j.jhazmat.2020.124885.

Supplementary Materials

Insights into processes and consequent metal(loid) behavior in dredged estuarine sediments upon electrokinetic treatment

Hussein J. Kanbar*, Mohamed-Tahar Ammami, Ahmed Benamar

Laboratoire Ondes et Milieux complexes (LOMC), UMR 6294 CNRS, University of Le Havre Normandy (ULHN), 76600 Le Havre, France. M-T. A, mohamed-tahar.ammami@univ-lehavre.fr; A.B: ahmed.benamar@univ-lehavre.fr

* Correspondence: Hussein J. Kanbar, hsen.kanbar@gmail.com, ORCID: 0000-0002-9505-9974

Published in Environmental Challenges

DOI: 10.1016/j.envc.2024.100880

Content

SM 1: Diffractograms of the materials that precipitated and settled in the anode (SA) and cathode (SC) chambers

The material that settled in the anode chamber (SA) was mainly composed of graphite and contained traces of brushite ($CaHPO_4.2H_2O$) and calcite ($CaCO_3$). The material that settled in the cathode chamber (SC) was mainly composed of hydrotalcite (Mg-carbonate), calcite ($CaCO_3$), and tri-sodium citrate.

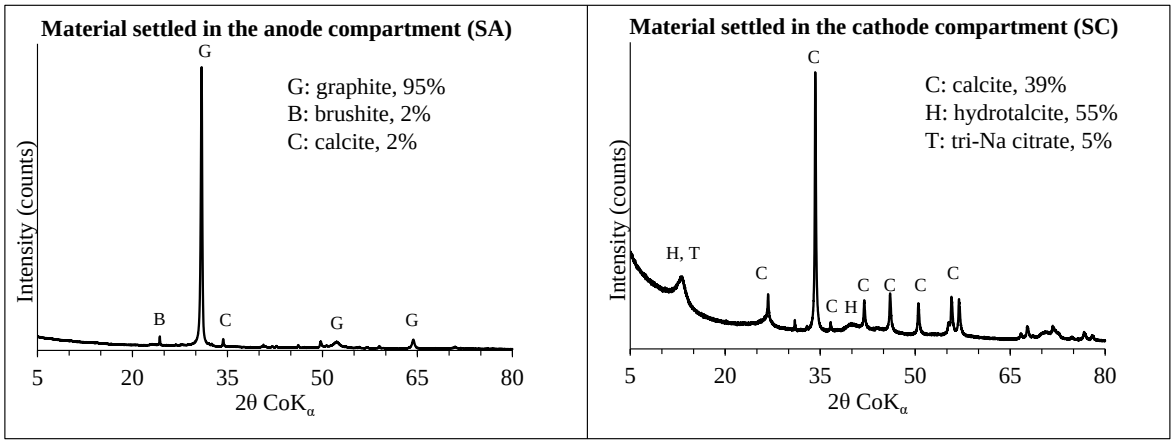

SM 2: Precipitation of gypsum on the surface of the sediment

Gypsum was found to have precipitated on the surface of the sediment (top ~2-5 mm) in the anodic zone (roughly between 0 and 20 cm away from the anode). Gypsum was also detected in foam samples that were collected above the anode chamber. The sediment samples presented in the main paper did not contain any gypsum, as confirmed by XRD measurements (Figure 6 in the main paper), since the top layer was removed before sampling (as discussed in section 2.3 in the main text). The diffractogram below shows the peaks that confirm gypsum presence in a surface anodic sediment. For the identification of all diffraction lines, the reader is referred to Figure 6 in the main paper.